Modelling Simul. Mater. Sci. Eng. **4** (1996) 409–419. Printed in the UK

Thermal transport across boundaries in diamond structure materials

W E Pickett, J L Feldman and J Deppe

Complex Systems Theory Branch, Naval Research Laboratory, Washington, DC 20375-5345, USA

Received 12 February 1996, in final form 5 May 1996

Abstract. Previous measurements of the thermal conductivity κ of chemical vapour deposition diamond films show values of κ near, or even exceeding, that of natural diamond in spite of the polycrystalline nature of the films. These data have led us to consider whether there can be a 'resonant' transfer of energy between identical crystallites separated by a material with different vibrational properties. We consider here a model of energy transfer between diamond-structure crystallites (Stillinger–Weber silicon) separated by a barrier region in which the mass is altered. We find that, for a pulse of energy deposited in one crystallite, there can be an efficient transfer of energy through the barrier region and subsequent build-up in a neighbouring crystallite if the vibrational spectrum of the barrier region is harder than that of the crystallites. If the vibrational spectrum of the barrier material is softer, the energy accumulation in the barrier region is at least as rapid as in the neighbouring crystallite and energy is retained longer in the region where it was deposited. The microscopic reasons behind this behaviour are discussed, and we conclude that the transmission probability between neighbouring crystallites leads to a more physical interpretation than a resonant transfer between next-neighbour crystallites.

1. Motivation

Because of the many extreme properties of diamond, the recent developments [1] in the growth of diamond films by chemical vapour deposition (CVD) have led to many expectations of commercial applications [2]. For the most part, such applications are still some years away. There is, however, immediate interest in one important type of application based on the high thermal conductivity of diamond, so-called 'thermal management' such as thermal spreaders for multichip modules to conduct the heat away as quickly as possible in a controlled manner.

Application of diamond films as thermal conductors was greatly stimulated by the remarkable finding by Graebner *et al* [3–5] that, although CVD diamond films are far from the ideal case of defect-free single crystals, nevertheless they conduct heat nearly as well as good natural diamonds or, for selected cases, even better. This result was, and is, remarkable when one considers the morphology of the films [1, 3]. Although CVD films show much variation depending on parameters of deposition, those with excellent thermal conductivity, κ, were (as are all films except homoepitaxial ones) crystallites separated by non-crystalline carbon. The crystallites tend to be long in the direction of growth (perpendicular to the film surface) and to be larger in the lateral direction near the top of the film (latest in the growth process).

The observation of good thermal conduction parallel to the film surface, in which the heat encounters boundary after boundary between crystalline diamond and non-crystalline C (and

0965-0393/96/040409+11$19.50

perhaps CH_x), stimulated the present work. One possibility for explaining the high κ might be called 'resonant heat transfer', in which thermal energy would be transferred efficiently between identical crystallites through a narrow region of lower thermal conductivity material. One can imagine normal modes of a polycrystalline film that have large amplitude in the crystallites and small amplitude in intervening material. Is it possible that, if one excites such modes in one crystallite the energy can be transferred through the intervening material to a neighbouring crystallite precisely because an identical vibrational spectrum and character (frequency and wavevector) are available?

In this paper we begin to address the question of heat transfer across interfaces, but adopt a simplified model and a molecular dynamics simulation. The model is described in section 2. In section 3 we present the results, and we discuss their possible implications for polycrystalline materials such as CVD diamond films in section 4.

2. Simulation model

We consider a diamond structure crystal of atoms whose interactions are described by the Stillinger–Weber (SW) potential [6], that is, Stillinger–Weber silicon. No doubt the SW parameters could be adjusted to provide an optimal description of diamond rather than Si, and more sophisticated models for carbon now exist [7]. For the purposes of our model study the specifics of the model should not be important. We do note that the potential includes anharmonicity, so we do not study a purely harmonic model. On the other hand, spot checks have indicated that in the calculations we report, the amplitudes are sufficiently small that anharmonicities play no role within the timescale we explore. The SW parameters and simulation procedures are those described previously [6, 8].

Rather than begin immediately with a system that includes structural changes across an interface, we have chosen to concentrate first on a model without structural disorder. Instead of a change in structure or force constants across the interface, we consider only variations in mass, and evaluate that effect alone. Such effects could in principle be studied experimentally by appropriate use of isotopic masses.

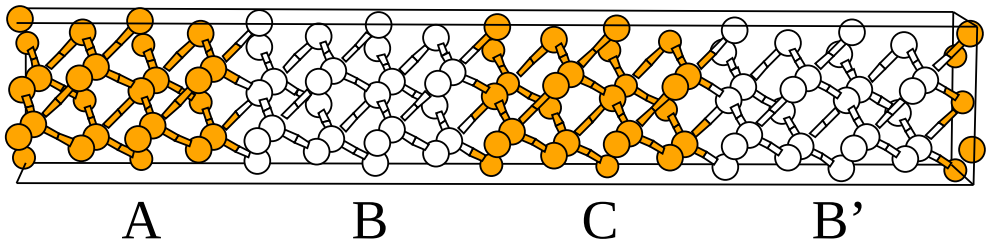

Figure 1. Schematic diagram of the simulation cell used in the MD calculations, with the regions labelled A, B, C, B′. Light and dark atoms indicate differing masses. The actual cell is $2 \times 2 \times 32$ cubes of the diamond structure (1024 atoms).

We treat a supercell of 1024 atoms with periodic boundary conditions in each of the three dimensions. The cell, shown schematically in figure 1, is a $2 \times 2 \times 32$ collection of cubic cells of the diamond structure, each containing eight atoms. Interfaces are taken to be perpendicular to the long (z) direction, with the masses taken to be $M_1 = 1$ in cubes 1–8 (region A) and cubes 17–24 (region C), while in cubes 9–16 (region B) and 25–32 (region B′) the mass M_2 is assigned various values. Since they are equidistant from the initial pulse of energy and have the same mass, the two regions B and B′ are physically but

not mathematically equivalent because of the randomness in the initial conditions. We will refer to them collectively as region B.

For the work we present here we introduce energy into a thin region in the centre of region A, either by beginning with displaced atoms at rest, or with undisplaced atoms with nonzero velocity. The displacements (or velocities) for the central plane in region A are chosen randomly in the $+z$ direction up to some maximum value z_{max} (or v_{max}). In the bordering atomic layers the displacements (velocities) are taken randomly from the interval $[-z_{max}/2, 0]$ ($[-v_{max}/2, 0]$). The change in centre of mass (net momentum) is small, and is set identically to zero by an equal displacement (velocity boost) of all atoms in the three layers. The randomness results in forces, and then displacements, in the x- and y-directions as well, making this a three-dimensional study as opposed to the one-dimensional studies on related systems that have been carried out previously [9]. We do, however, monitor the energy dispersion in the z direction only.

For the purpose of analysis the energy was designated to individual atoms in the same fashion as done in a previous calculation by Kluge *et al* [10] of the thermal conductivity of amorphous silicon within the Green–Kubo theory. In particular, the three-body potential energy terms of the Stillinger–Weber potential were divided among the three involved atoms as 1/2, 1/4, and 1/4 with the 1/2 designated to the apex atom, and the two-body term was split equally between interacting atoms.

Throughout this paper we express quantities in the natural units for the SW potential. For the Si parameters we adopt, these are: length, $l = 0.209\,51$ nm; time, $\tau = 7.66\times10^{-14}$ s; energy, $\epsilon = 2.167$ eV; velocity, $v = l/\tau = 2.73 \times 10^5$ cm s^{-1}; mass $M_1 = 28.09$ amu.

3. Results

In figure 2 we show a series of surface plots in time (t)–z-direction space. The height of the surface at a given point (z, t) is proportional to the average energy per atom in that atomic layer of the supercell (there are eight atoms in each such atomic layer). The peak at $t = 0$ in the vicinity of unit cell 4 reflects the initial 'thermal spike' prepared in the centre of the unit mass region A. This peak corresponds to a maximum initial displacement of $z_{\max} = 0.025l \approx 0.05$ Å. The time step is chosen as $0.005\tau = 3.8 \times 10^{-4}$ ps as used previously [8]. We display 4000 time steps, since that is sufficient to indicate the behaviour we will concentrate on.

The surface plots in figure 2 for mass $M_2 = 0.5$, 1.0 and 2.0 are representative of results we have observed for a variety of mass ratios (see below for a listing of simulations). For a ratio of unity, i.e. a reference homogeneous crystal, the energy spreads smoothly until the disturbance fronts collide (owing to the supercell periodicity). As the simulation proceeds, the energy distribution over the cell is clearly tending to a uniform value, although after the 4000 time steps shown there are still strong transient energy fluctuations.

For $M_2 = 2$ the disturbance is strongly reflected and remains confined to region A. A small amount of energy is transmitted and, on a higher resolution plot, the decrease in velocity of the disturbance in region B is clear. For the time of this simulation, and even for considerably longer times, very little energy is transmitted through region B into region C.

For $M_2 = 0.5$ the increase in velocity of the disturbance front is visible at the A–B boundary. After time step ~ 2000, however, it is evident that the average energy density in region C (mass M_1) is becoming much higher than in region B (mass M_2) through which the energy was transferred. Extension of the simulation to longer times indicates that the energy density in region C approaches that of region A while that in region B remains much lower. After much longer times, of course, the energy will finally equalize.

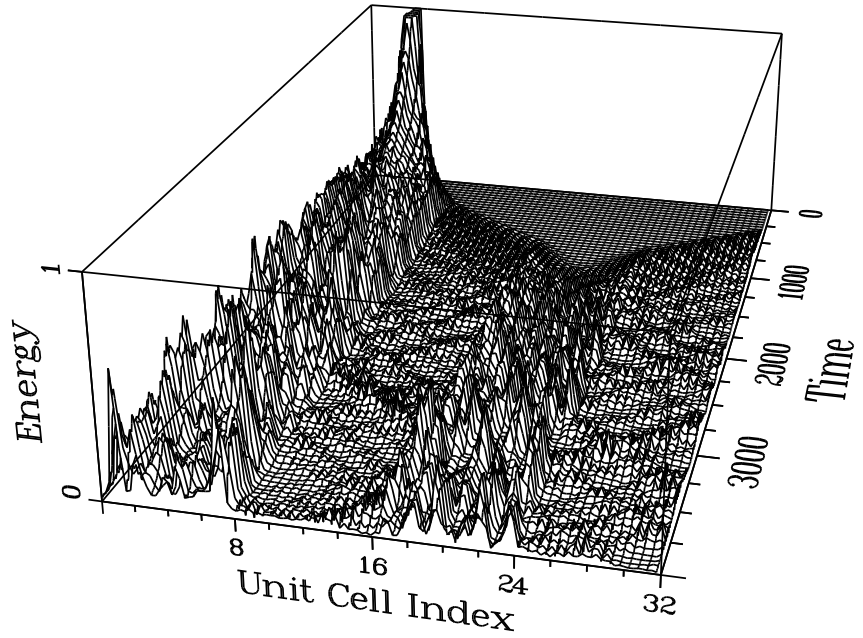

(*a*)

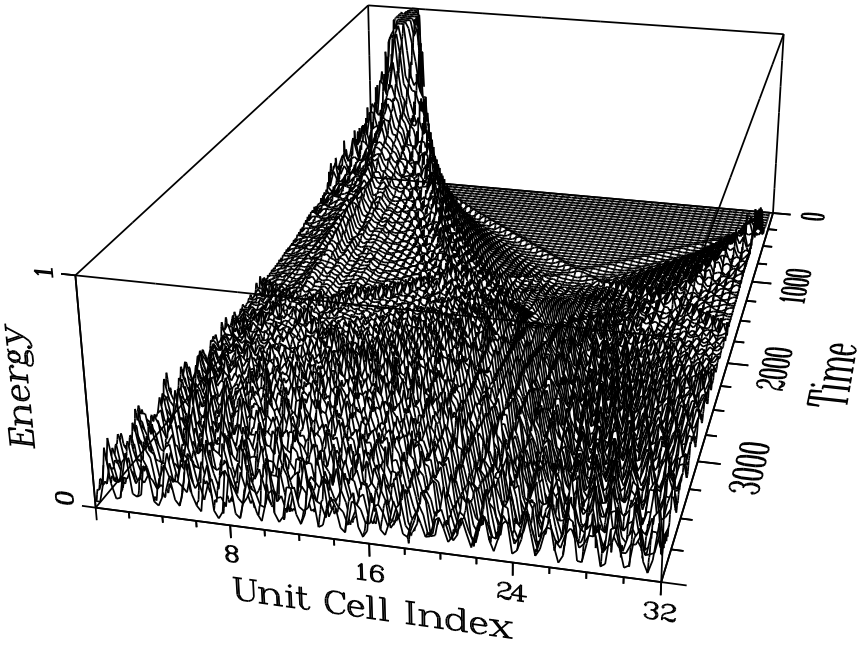

(*b*)

Figure 2. Surface plot of the average energy per x–y layer in (z–t) space, for masses $M_1 = 1$ and $M_2 = 0.5$ (*a*), 1 (*b*) and 2 (*c*). The energy pulse (truncated in height for plotting purposes) is deposited (rear of figure) in the centre of region A (around unit cell index 4) and spreads as described by classical dynamical calculations. Regions B and B′ are the cells 8–16 and cells 24–32, respectively. Cells 16–24 form region C.

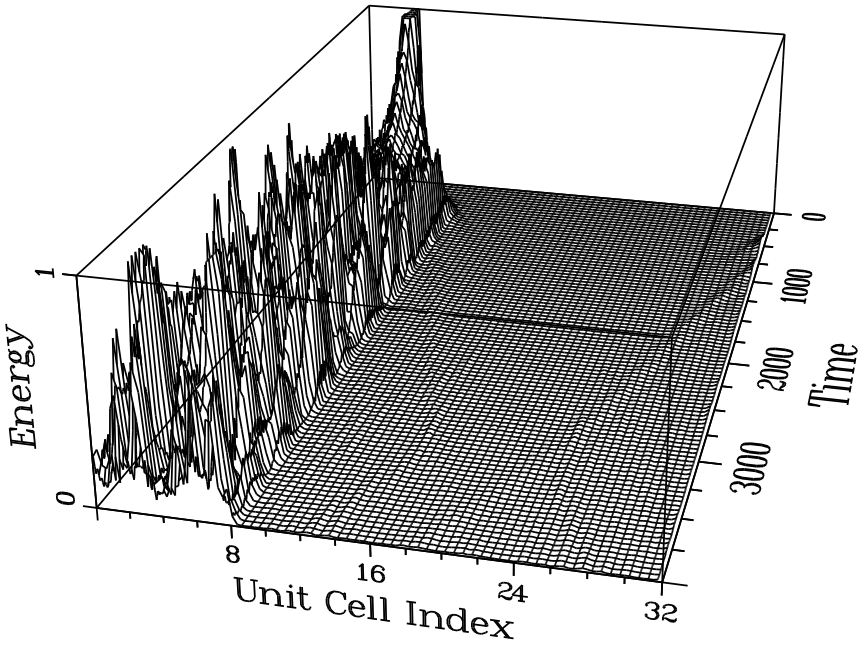

(*c*)

Figure 2. (Continued)

The salient results of the simulations can be seen by plotting the average energy/atom in each of regions A, B, and C versus time, as done in figure 3. The energy is initially entirely in region A; it begins to be transferred into the bounding region B after ~ 1000 time steps (when the disturbance front reaches the boundary), and it reaches region C later, at a time depending on the mass ratio.

The results can be summarized rather succinctly. If $M_2 \leqslant 1$, energy is transferred through region B (of lighter masses than in region A) and the energy density in region C rapidly becomes comparable to that in region A where the disturbance originated. This occurs for $M_2 = 1/2$ in spite of the fact that the energy in region B remains at a much lower level: the energy is not simply distributed but is transferred through the low mass region. However, if $M_2 > 1$ the energy is effectively trapped within region A for a comparatively long time. We have shown in figure 3 the region-averaged plots corresponding to the simulations shown in figure 2, except that they are extended to 2×10^4 time steps $= 7.6$ ps. We have not pursued the question of the amount of time necessary for the energy to equilibrate throughout the cell, except to note that there is no significant change in energy distribution on a timescale ≈ 5 times that shown in figure 3 (10^5 time steps $= 38$ ps). We have observed this phenomena for a variety of masses spanning the range $0.1 < M_2 < 2$.

An interesting question then is: how close must the mass ratio be to unity before this transmission or reflection of energy becomes insignificant? Figure 4 shows the energy distribution versus time for $M_2 = 0.95$, 0.98, 1.02 and 1.05. For comparison, see the $M_2 = 1$ plot, figure 3(*b*): after 15 000 time steps the energies in regions B and C are equal within the level of fluctuations, although they are still slightly below that in region A. Even for $M_2 = 0.98$ the energy in region C approaches that within region A to within perhaps 10% while that in region B is $\approx$ 30–35% less than in region A. For $M_2 = 1.02$, after

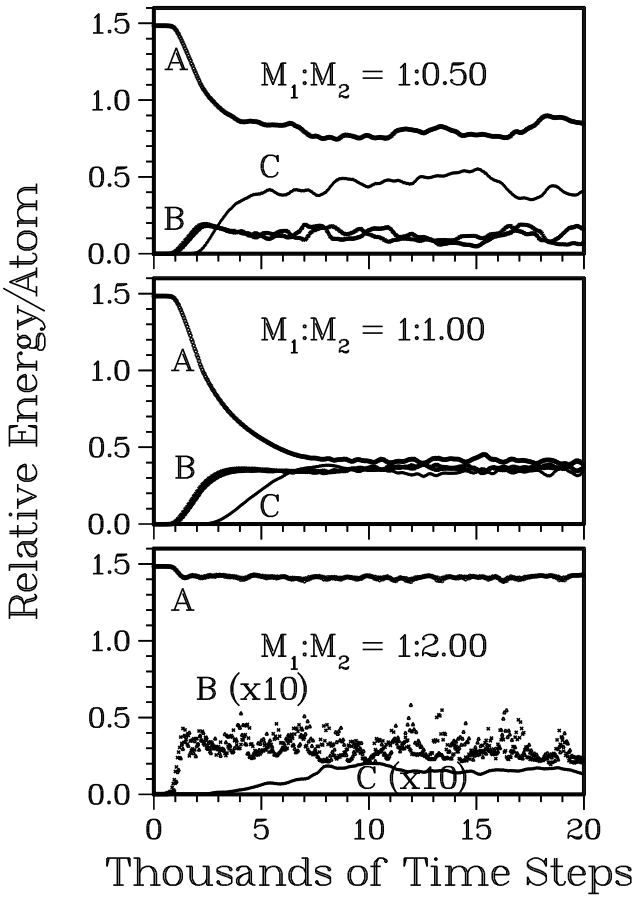

Figure 3. Average energy in regions A, B, and C versus time, for masses $M_2 = 0.5$, 1.0 and 2.0 (see text). The upper panel corresponds to the simulation shown in figure 2.

15 000–20 000 time steps, ≈ 45% of the energy is still 'blocked' within region A (25% of the volume).

4. Discussion

4.1. Dependence on initial conditions.

The results of simulations such as those discussed here are somewhat dependent on the choice of the initial energy pulse. For the cases we have presented, for which atoms in three layers only are excited, there is no important difference whether the energy is deposited by giving a displacement or by giving an impulse. We have looked at analogous MD simulations in which the initial energy is distributed over 16 atomic layers (144 atoms, the inner half of region A), which we will call type 2 initial conditions, rather than the case discussed above (three layers, involving 24 atoms), our type 1 initial conditions. Even for the $M_2 = 1$ case (i.e. no barrier) shown in figure 5, the results were quite different. This difference can be viewed as a distinction between the energy pulses 'injected' by the initial conditions. Considering the expression for atomic displacements (or velocities) in terms

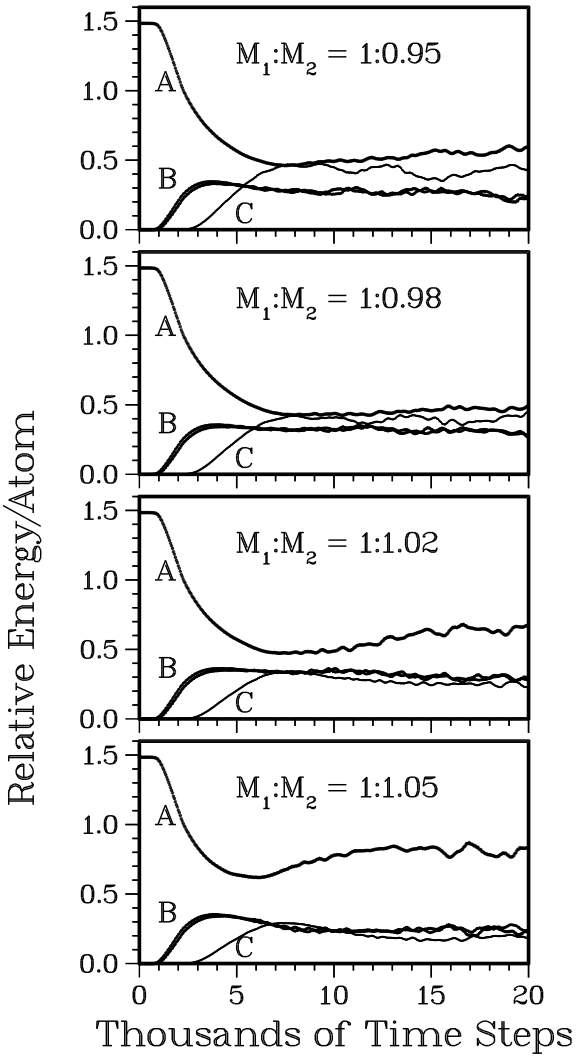

Figure 4. Average energy in regions A, B and C versus time, for masses $M_2 = 0.95$, 0.98, 1.02 and 1.05. Note that even small changes in the vibrational spectrum (i.e. the relative mass) can affect the energy transport substantially.

of phonon normal modes, the less localized pulse is expected to involve relatively many small wavevector (Q), low-frequency phonons, and therefore resembles more closely a heat pulse. Since small Q modes are dispersionless and energy packets propagate also without dispersion for such modes, it is plausible that there is less rapid change in the shape of the energy pulse. We have examined this question in some detail.

4.2. Distribution of injected phonons.

By our choice of initial conditions we have 'injected' a pulse of normal mode vibrations, the distribution and relative phases of which can be obtained by inverting the initial displacements or velocities. Although SW-silicon represents the spectrum of silicon

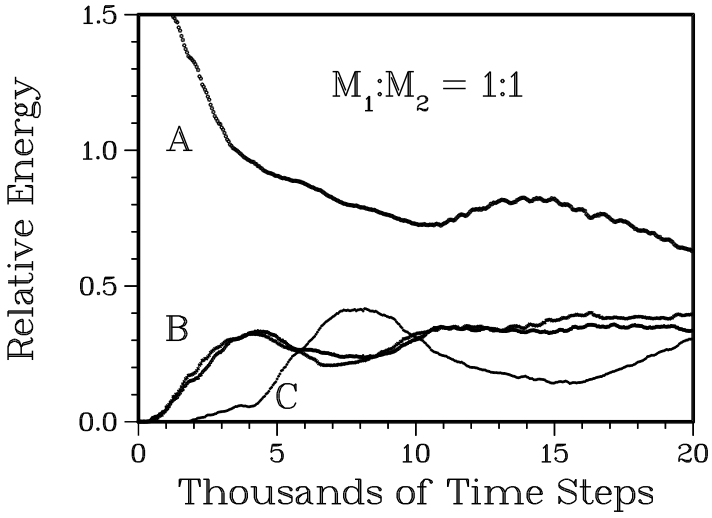

Figure 5. Energy dispersion results analogous to figure 3 (central panel) except that 144 atoms were displaced instead of 24 atoms. Note that the energy has not equalized over the cell after 20 000 time steps.

reasonably well, our choice of supercell with 1024 atoms and periodic boundary conditions imposes some restriction on the dynamical behaviour that is allowed.

The dynamical matrix at $Q = 0$ (i.e. for periodic boundary conditions) for $M_2 = 1$ was set up and diagonalized to obtain the frequencies and eigenvectors of the normal modes. In the top panel of figure 6 the normal mode frequency distribution at $Q = 0$ is shown for our supercell. Compared with crystalline Si, it is evident from figure 6 that the density of low-frequency modes is small. This is due to the fact that in two directions the supercell is only two lattice constants long, so there are no long wavelength modes in those directions.

In the upper panels of figures 6(*a*) and (*b*) the relative population of modes versus frequency is pictured for the two types (1 and 2) of initial conditions. As expected, the excitation of low-frequency modes is several times higher when the initial energy pulse is distributed over a wider region. An example of one run for the $M_2 = 1$ case (equal masses, no boundaries) is shown in figure 5. Whereas for the type 1 initial conditions the energy is equally spread ($\pm 10\%$) over the regions A, B, and C after $\approx 8 \times 10^3$ time steps, for the type 2 initial conditions there is still a factor of two variation after 2×10^4 steps. From figure 5 one might estimate that it would require 3–4 $\times 10^4$ time steps to obtain (near) equidistribution of energy throughout the supercell.

4.3. Relation to previous work

In their theoretical treatment of Kapitza resistance associated with a planar boundary between two solids, Young and Maris (YM) [11] considered the scattering of incident plane waves. They define the spectral function,

$$F(\omega) = \hbar\omega n(\omega, T)G(\omega)V_z t(\omega)$$

for the rate of transmitted vibrational energy across the boundary. The phonon density of states is denoted by G, n is the Bose–Einstein thermal occupation function, v_z is the group velocity perpendicular to the interface, and $t(\omega)$ is an averaged transmission coefficient for

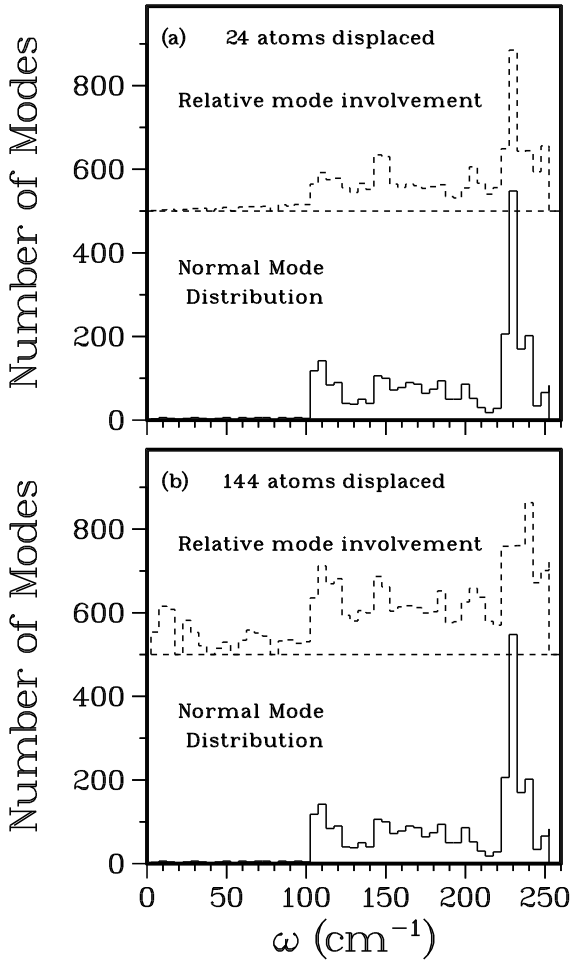

Figure 6. The normal mode distribution at the zone centre in the supercell (lower part of each panel), compared with the distribution of normal mode excited by the displacements of three atomic layers containing (*a*) 24 atoms and (*b*) 144 atoms. The scale gives the number of modes in 10 cm^{-1} bins for the lower curve, whereas the upper curve in each panel has been normalized arbitrarily to allow comparison.

an incoming mode of frequency ω. While YM were considering a very different situation than ours it appears that there is some relationship between the two. We can consider our initial energy pulse to be a superposition of normal modes within the slab we are considering; e.g. initially, partition A. Our results could be compared to a YM type theory in more detail. To do that one would use the YM function but with $\omega n(\omega, T)G(\omega)$ replaced with the distribution function corresponding to our energy pulse and with the use of the SW potential and the diamond structure rather than the spring force constant model and fcc structure of YM.

While we have not performed the above analysis, it is interesting to analyse qualitatively our results in terms of the YM results since the SW potential is very short-ranged as was the YM force constant model. Let us first consider energy propagation into region B for the case $M_2 = 2$ (see figure 2(*c*) and figure 3 (lower panel)). Then the transmission coefficient

$t(\omega)$ is zero for the portion of the spectrum in A not appearing in B due to the larger mass of B; the energy in that portion of the spectrum is totally reflected at the A–B boundary and is trapped (within the harmonic approximation). On the other hand since the energy that enters B is of a spectral range included in A then it can traverse the B–C boundary, i.e. the transmission coefficient for B to C is non-zero for the full spectral range of B, so there is no trivial entrapment of energy. Effects of multiple reflections at boundaries will arise in our simulations because of our periodic boundary conditions, and they are not easily identified and separated out. Next, consider the case $M_2 = 0.5$ of figures 2(a) and 3 (upper panel). The fact that A loses only about the fraction $0.7/1.5 \approx 0.5$ of its energy through both A–B boundaries can be explained by the approximately constant value of $t(\omega)$ (≈ 0.5, see the curve $K' = 1$ in figure 6 of YM). The large build-up in energy in C can be understood in terms of $t(\omega)$ in the YM model. From B ($M = 0.5$) to C ($M = 1$) the relevant $t(\omega)$ values are given by the $K' = 1$ curve in figure 8 of YM, and the initial spectrum (in B) is the spectrum transmitted from A. As shown in that figure, $t(\omega)$ is close to 1 for $0.5 \leqslant \omega \leqslant 1.3$, drops down to less than 0.4 for $\omega \geqslant 1.5$, and finally goes to zero at the maximum frequency $\omega_{max} \approx 2$. If it is assumed that $t(\omega)$ remains near unity down to the lowest frequencies, then a large fraction of the spectrum is transmitted from B to C with a transmission coefficient near unity. This circumstance, coupled with a significant reflection (i.e. $t(\omega) \approx 0.5$) at the C–B boundary, leads to the large build-up of energy in C.

Finally, we note one other feature relating to initial conditions. A vibrational energy transport study recently was reported [9] on ordered and disordered linear chains in the harmonic approximation. After many periods of the maximum frequency, the energy distribution was compared for the impulse and for the displacement initial conditions, where a single atom was perturbed initially. The distributions were qualitatively different: the impulse initial condition yielded a rather sharp energy front determined by the sound velocity, whereas the displacement initial condition gave a broad distribution that extended up to the sound velocity front. We have observed a distribution with a sharper 'sound' velocity front [12] for the momentum initial conditions than for the displacement conditions but, as mentioned earlier, our results for the temporal distribution of energy do not differ greatly between the two sets of initial conditions. Ours is a more incoherent energy insertion and the normal mode distribution of our system is also quite different from that used for the one-dimensional chain [9].

5. Summary

Using molecular dynamics simulations we have found (figure 4) that energy transfer through an abrupt interface can be strongly affected by seemingly small differences in the dynamical properties of the two regions. (Preliminary calculations that introduce mass disorder over a few layers at the interface do not show significant difference.) The results do depend, however, on the way the heat pulse is prepared: a pulse initially spread over a 16 atomic layer region disperses somewhat differently than one initially spread over only four atomic layers.

Our discussion in the previous section has been couched in idealized terminology: regions A and C were interpreted to have a frequency spectrum characteristic of the bulk with mass M_1, whereas the regions B and B$'$ were interpreted as representative of the bulk crystal with mass M_2. This is an oversimplified picture. Actually, atoms within a few atomic layers of the interface will not have a frequency spectrum corresponding to any bulk crystal, but will experience the presence of both masses. Interface modes may occur; however, they will not be excited by our choice of initial conditions so they should not be

important in the interpretation of our simulations. In addition, many more of the model parameters could be varied than we have done in this study.

Further work may proceed in new directions. Another way to address the question we posed in the introduction would be to dispense with the periodic supercell, and rather evaluate the transmission coefficient for vibrational waves impinging from a semi-infinite region A of mass unity, encountering finite region B of mass M_2, and continuing on into semi-infinite region C of unit mass. Alternatively, one can alter the periodic system, either by introducing disorder into one or more of the regions, or by introducing force constant disorder rather than mass disorder.

Acknowledgments

We have benefitted from discussions with P B Allen. We thank J Q Broughton for the use of his molecular dynamics codes, and M Sadd for use of codes to calculate the eigenfrequencies. JD acknowledges the support of the National Research Council Research Fellowship.

References

[1] See, for example, the reviews by; Celli F G and Butler J E 1991 *Ann. Rev. Chem.* **42** 643
Spear K E and Frenklach M 1993 *Synthetic Diamond: Emerging CVD Science and Technology* ed K E Spear and J P Dismukes (New York: Wiley) p 243
[2] Yoder M 1993 *Synthetic Diamond: Emerging CVD Science and Technology* ed K E Spear and J P Dismukes (New York: Wiley) p 3
Angus J C, Wang Y and Sunkara M A 1991 *Rev. Mater. Sci.* **21** 221
[3] Graebner J E, Jin S, Kammlott G W, Herb J A and Gardinier C F 1992 *Nature* **359** 401; *Appl. Phys. Lett.* **60** 1576
[4] Graebner J E, Hartnett T M and Miller R P 1994 *Appl. Phys. Lett.* **64** 2549
[5] Reviews have been given by Graebner J E 1993 *Diamond Films and Technol.* **3** 77
Morelli D T 1994 *Chemistry and Physics of Carbon* ed P A Thrower (New York: Marcel Dekker) pp 45–109
[6] Stillinger F H and Weber T A 1985 *Phys. Rev.* B **31** 5262
[7] Brenner D W 1990 *Phys. Rev.* B **42** 9458
[8] Broughton J Q and Li X P 1987 *Phys. Rev.* B **35** 9120
[9] Zavt G S, Wagner M and Lutze A 1993 *Phys. Rev.* E **47** 4108
Wagner M *et al* 1992 *Phil. Mag.* **65** 273
[10] Kluge M, Feldman J L and Broughton J Q 1993 *Phonon Scattering in Condensed Matter* vol VII, ed M Meissner and R O Pohl (New York: Springer) p 225
[11] Young D A and Maris H J 1993 *Phys. Rev.* B **40** 3685
Stoner R J and Maris H J 1993 *Phys. Rev.* B **48** 16 373
[12] The elastic constants for the SW potential given by E R Cowley 1988 *Phys. Rev. Lett.* **60** 2379 are consistent with our simulations.